RSC Advances

PAPER

View Article Online
View Journal | View Issue

Cite this: *RSC Adv.*, 2017, **7**, 54091

A DFT study of $(WO_3)_3$ nanoclusters adsorption on defective MgO ultrathin films on Ag(001)

Hui Zhang,[a] Jia Zhu,*[a] Zhenxing Fang,[c] Xianglan Xu,[d] Yongfan Zhang*[b] and Yuehua Fan[a]

The structures and electronic properties of $(WO_3)_3$ nanoclusters adsorption on defective MgO ultrathin films on Ag(001) have been investigated by means of density functional theory (DFT) calculations including dispersion interactions. Our results show that, after deposition, the oxygen vacancy on the defective MgO/Ag(001) films is healed by one terminal oxygen atom of the $(WO_3)_3$ clusters through forming four O–Mg bonds. The conformation of the $(WO_3)_3$ nanoclusters is distorted slightly and the W_3O_3 cyclic conformation of adsorbed $(WO_3)_3$ nanoclusters is still maintained. The defective MgO/Ag(001) 2D films lead to enhancement of the adsorption energy between the $(WO_3)_3$ clusters and the substrates, compared to that on defect-free MgO/Ag(001) 2D films and a defective MgO(001) surface. It is interesting that obvious charge transfer (2.74*e*) occurs from the defective MgO/Ag(001) films to the 5d empty state of the $(WO_3)_3$ clusters, which mainly originated from spontaneous electron tunneling through the thin MgO dielectric barrier, and less from the surface defective state as the consequence of the formation of O–Mg adsorption dative bonds at the interface. In addition, compared with $(WO_3)_3$ nanoclusters in the gas phase, on the defect-free MgO/Ag(001) 2D films and the defective MgO(001) surface, different scanning tunneling microscopy images and vibrational spectra for depositing $(WO_3)_3$ nanoclusters are observed, which could help in the identification of $(WO_3)_3$ nanocluster adsorption on the defective MgO/Ag(001) ultrathin films in future experiments. As a consequence, our results reveal that $(WO_3)_3$ nanoclusters adsorption on defective MgO/Ag(001) ultrathin films provide a new avenue to tune and modify the charge state and chemical reactivity of tungsten oxide nanoclusters.

Received 7th October 2017
Accepted 18th November 2017

DOI: 10.1039/c7ra11025a

rsc.li/rsc-advances

1. Introduction

Early transition metal oxides are of great technological importance due to their wide applications in catalysis, sensors, electrochromic devices, *etc.*[1–3] Among them, increasing interest has been devoted to tungsten oxide, which has been found to accelerate many types of reactions,[4] such as alkane isomerization,[5] alkene metathesis,[6] alcohol oxidation,[7] and selective NO reduction.[8] In recent years, tungsten oxides loaded on different supports such as TiO_2,[9,10] Cu–O[11] and FeO/Pt(111)[12] by direct sublimation of WO_3 have been extensively studied in an attempt to correlate the structure with catalytic performance, like dehydration of 2-propanol,[13] oxidation and reduction of aliphatic alcohols,[14] or polymerization of formaldehyde[15] and acetaldehyde,[16] which has suggested that the catalytic properties of tungsten oxides are strongly influenced by the support. Therefore, a detailed characterization of the structures and electronic properties of the supported oxide catalysts is essential for a rational design of new catalytic materials.[17,18]

Many experiments have proved that the catalytic characterization at atomistic level of supported tungsten oxide is strongly depended by some of key factors, including the diverse nature of support defects, quantum size effects and the form of the supported material (powder, thin films, single crystal), *etc.* Di Valentin *et al.*[19] have shown that when $(WO_3)_3$ clusters supported on reduced TiO_2 surfaces, the defective support donates one electron to the $(WO_3)_3$ clusters. Thus make singly charged $(WO_3)_3$ clusters activating linear radical chain polymerization of formaldehyde with very low activation barriers. Recently, we have also reported detailed theoretical investigations on $(WO_3)_3$ nanoclusters deposited on the defective MgO(001) surface with three kinds of F_S centers (F_S^0, F_S^+, and F_S^{2+}), and our results indicated that the structural changes of $(WO_3)_3$ clusters are well correlated with various electron donor ability of the defective surface, which are helpful in the interpretation of the mechanism of formation of various $(WO_3)_3$ structures on different surfaces.[20] Furthermore, except that introducing diverse nature of support defects, a continuously increasing interest has also been devoted to another form of the support material, ultrathin

[a]*College of Chemistry and Chemical Engineering, Jiangxi Normal University, Nanchang, Jiangxi 330022, China. E-mail: jia_zhu@jxnu.edu.cn*
[b]*Department of Chemistry, Fuzhou University, Fuzhou, Fujian, 350108, China. E-mail: zhangyf@fzu.edu.cn*
[c]*Department of Physics, Zunyi Normal University, Zunyi, Guizhou, 563006, China*
[d]*Institute of Applied Chemistry, College of Chemistry, Nanchang University, Nanchang, Jiangxi, 330031, China*

oxide films grown on metal substrates, to control the configurations and electronic properties of the monodispersed oxide clusters.[21–26] These systems exhibit unusual chemical and electronic properties with respect to thicker films or single crystal oxide surfaces, due to the presence of the dielectric boundary and the reduced dimensionality of the insulating films, offering new opportunities for the design of new functional materials.[27–30] One specific and crucial property of ultrathin oxide films is the occurrence of a spontaneous charge transfer from the metal support to an adsorbed species through the thin insulating layer (or *vice versa*).[24,28,31–35] This has been done recently for various systems, including adsorbed Au atoms,[36,37] Au clusters,[38–40] $(WO_3)_3$ clusters,[34] or simple molecules like O_2,[41] NO_2 [35,42] when adsorbed on MgO/Ag(001) films becoming negatively charged. Therefore, the possibility to grow or deposit monodispersed oxide clusters on different kinds of supports with diverse nature of defects and the forms of the supported material (thin films, single crystal) open new scenarios for the understanding of the fundamental properties of these systems. The control of reactivity for tungsten oxide clusters supported on defective surface, as well as the perfect films has been explored in our previous studies.[20,34] However, up to now little information is discussed for the atomic structure and electronic properties of tungsten oxides supported on defective films which appear to be more complicated, in which the interaction between the clusters and defective films materials needs to be considered. Therefore, it is interesting and appealing to further investigate the effect on the $(WO_3)_3$ clusters adsorbing on the defective MgO ultrathin films supported on metal substrate and whether they will exihibit different and unique structures and charge states, with respect to that deposition on defective crystal MgO(001) surface and perfect MgO/Ag(001) ultrathin films, which is essential for the rational design of new nanostructures.

In this paper we present a detailed DFT study on the configurations and electronic structures of $(WO_3)_3$ clusters supported on the defective MgO ultrathin films supported on Ag(001) including dispersion interactions. We first use the *ab initio* molecular dynamic (MD) method to sample possible configurations of this complicated multidimensional system, the most stable structure is determined by further geometrical optimizations, and the electronic properties of $(WO_3)_3$ clusters supported on the defective MgO/Ag(001) films are discussed with particular attention to cluster–support interaction effects in terms of electronic modifications of the clusters. Finally, we predict the STM images and vibrational spectra, which can help in the identification of the formation of $(WO_3)_3$ nanoclusters adsorption on the defective MgO/Ag(001) ultrathin films in future experiments. Our theoretical works can provide deep insight into the properties of this well-defined model system and open new perspectives for the design and study of model catalysts and their activity as a function of structure and charge state.

2. Computational details

First-principles calculations based on density functional theory (DFT) were carried out utilizing the Vienna ab initio simulation package (VASP)[43–45] and the projector augmented wave (PAW) method.[46,47] The generalized gradient approximation of the exchange–correlation functional proposed by Perdew–Wang (PW91) was employed,[48] and the kinetic cutoff energy for the plane-wave expansion was set to 400 eV. The choice of the PW91 functional was suggested by the possibility to directly compare results of this study with those of similar systems investigated previously.[18,30,31,34] Spin polarization has been considered. The MgO/Ag(001) substrate was modeled by four metal layers (two layers for *ab initio* molecular dynamics (AIMD) simulations), and a three-layer (3ML) MgO films was deposited on top of it. The oxygen vacancy called an F center created by removing a neutral O atom from the surface. As expected, it can be seen clearly that the electronic density localized in the oxygen vacancy region (Fig. 3a). The experimental lattice constant of Ag (4.09 Å) is 3% smaller than that of MgO (4.21 Å). In the calculations, the optimized Ag and MgO lattice parameters are 4.16 and 4.25 Å, respectively, and the lattice mismatch is reduced to about 2%. Therefore, the MgO layers are slightly contracted with respect to their bulk distance after they were supported on the Ag metal. During the geometry optimization of MgO/Ag(001) interface, all atoms in the MgO films and in the two outmost Ag layers were relaxed while the remaining two Ag layers were fixed to their bulk position (in the AIMD simulations only the atoms of the top Ag layer were relaxed). To avoid interactions between neighboring $(WO_3)_3$ clusters, a (5×5) supercell of defective MgO/Ag(001) films consisting of 249 atoms (100 Ag, 75 Mg, and 74 O atoms) was employed, and a $(3 \times 3 \times 1)$ Monkhorst–Pack was used for the *k*-point sampling. The role of the vdW interaction was investigated using DFT-D2 method including the pairwise force field implemented by Grimme.[49]

The structures and the electronic properties of $(WO_3)_3$ clusters and its anions has been already discussed in the literature.[50–52] It is well known that, $(WO_3)_3$ clusters shows unusual stability and is the major species in the tungsten oxide vapor. The ground state of $(WO_3)_3$ clusters possesses a coplanar W_3O_3 cyclic conformation (3.53 Å in W–W distance) with D_{3h} symmetry (see Fig. 1a). The bond lengths of W–O and W=O are 1.91 and 1.73 Å, respectively. It is noted that the lowest unoccupied molecular orbital of $(WO_3)_3$ cluster is mainly consists of the tungsten 5d orbital, occupation of this orbital by adding one or two electrons leads to a considerable shortening of the W–W bond length relative to the neutral $(WO_3)_3$ structure (3.24 Å in $[(WO_3)_3]^-$ and 3.07 Å in $[(WO_3)_3]^{2-}$), due to the formations of the strong three-center, one-electron and three-center, two-electron metal–metal bonds, respectively.[52]

Compared with the cases of metal nanoparticles that have been extensively studied,[53–55] the deposition of oxide clusters on the solid surfaces is more complicated. Since there are many possible arrangements of the $(WO_3)_3$ clusters on the defective MgO/Ag(001) ultrathin films, special effort has been paid to investigate the adsorption configuration of $(WO_3)_3$ clusters on the defective MgO/Ag(001) ultrathin films. In order to find the most stable configurations of the deposited $(WO_3)_3$ clusters as much as possible, and reduce the influence of artificial factors, first-principles *ab initio* molecular dynamics (AIMD) simulations using the Nosé algorithm[56] were used to explore possible

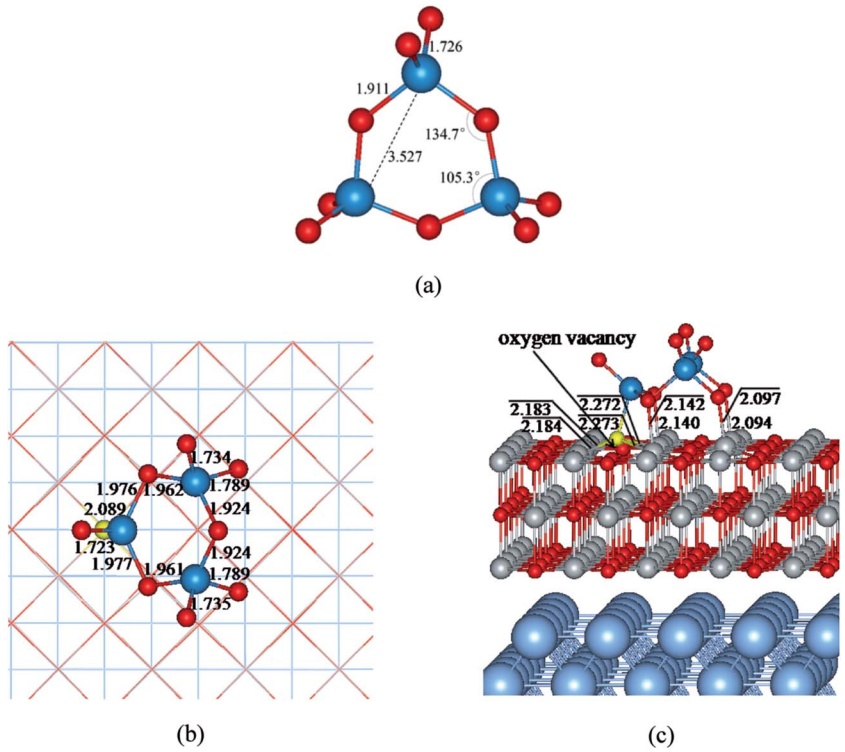

Fig. 1 Optimized ground state structures of (a) gas phase $(WO_3)_3$ clusters (top view); (b and c) $(WO_3)_3$ clusters deposition on the defective MgO ultrathin films supported on Ag(001) (top and side views). W, O, Mg, and Ag atoms are denoted by dark blue, red, gray, and light blue spheres, respectively. For emphasis, the yellow sphere represents the terminal O atom of $(WO_3)_3$ clusters that is used to heal the oxygen vacancy on the surface. The lengths of the bonds at the interface labeled in figures are in angstrom.

adsorption configurations using a low cutoff energy (200 eV). The simulation time was 10 ps with a time step of 1 fs at the temperature of 600 K. Then possible adsorption configurations were sampled from the results of the MD simulation every 50 steps, resulting in 200 initial structures for each MD process. Finally, further structural optimizations were carried out to determine the most stable adsorption configurations using more accurate settings (see above). The results of previous studies[34,57,58] demonstrate that adopting the method of *ab initio* molecular dynamics combining with quantum mechanics to determine the configuration of complex systems is feasible.

3. Results and discussion

3.1 Structures of the $(WO_3)_3$ nanoclusters on the defective MgO ultrathin films supported on Ag(001)

The most stable structure of $(WO_3)_3$ nanoclusters supported on the defective MgO/Ag(001) ultrathin films is shown in Fig. 1c, and for clarity, the top view of $(WO_3)_3$ fragment is provided in Fig. 1b. It can be seen clearly that the oxygen vacancy on the MgO ultrathin films is healed by one terminal oxygen (O_t) atom of the $(WO_3)_3$ nanocluster through forming four O_t–Mg bonds with the bond length in the range of 2.18–2.27 Å. At the same time, another two terminal (O_t) and two bridging (O_b) oxygen atoms are bonded to surface Mg atoms forming bonds of about 2.10 Å length. This leads to a total of eight adsorption bonds formed at the interface. The corresponding adsorption energy is 5.84 eV (see Table 1), which is 2.36 eV and 0.08 eV higher in energy than that on the defect-free MgO/Ag(001) films (3.48 eV) and thick defective MgO(001) surface (5.76 eV) reported in previous works, respectively.[20,34] It is suggested that the defective MgO/Ag(001) 2D films lead to enhance adsorption energy and stronger interaction between the $(WO_3)_3$ clusters and the substrates, compared to that on the defect-free MgO/Ag(001) 2D films and the defective MgO(001) surface. Not surprisingly, the strong interaction results in a significantly change of the supported clusters. Compared to $(WO_3)_3$ cluster in gas phase, the W_3O_3 cyclic structure is still maintained. But the conformation of $(WO_3)_3$ part is obvious distorted: the W–W distances decreased from 3.5 Å to 3.0 Å. One W atoms is 1.9 Å lower than the other two W atoms, and two O_b atoms significantly deviate from the cyclic plane, so that three W atoms and three O_b atoms of the clusters are no longer coplanar. An approximate symmetry plane through the lowest W atom and the opposite bridging O atom is observed. In addition, significant elongation of two W–O_b bonds in which the O_b atoms are coordinated with the surface Mg atoms are observed (about 2.0 Å). Then, we discuss the surface rumpling for the dielectronic layer at MgO/Ag(001) interface and the relaxation for the top layer of the MgO films. For the clean defective MgO(3ML)/Ag(001) ultrathin films, the MgO/Ag(001) interface distance away from the oxygen vacancy is 2.71 Å, which is in good agreement with the previous results.[59–61] And the interface distance near the oxygen vacancy is slightly increased (2.74 Å). While after the $(WO_3)_3$ clusters

Table 1 Adsorption energy (E_{ads}), net Bader charge (q), work function change ($\Delta\phi$), interface distance (d) and the distances of W–W for $(WO_3)_3$ clusters deposited on 2ML and 3ML defective MgO films supported on Ag(001). The values in the parentheses are obtained by DFT-D2 method

System	E_{ads}[a] (eV)	q[b] (e)	$\Delta\phi$ (eV)	d (Å)	W–W distances (Å)
$(WO_3)_3$/F_s-MgO(3ML)/Ag(001)	5.84(7.49)	−2.74(−2.78)	0.53(0.63)	2.66(2.50)	3.06, 2.91, 2.91(3.07, 2.92, 2.93)
$(WO_3)_3$/F_s-MgO(2ML)/Ag(001)	5.60(7.33)	−2.69(−2.75)	0.80(0.83)	2.67(2.50)	3.06, 2.90, 2.90(3.08, 2.92, 2.92)

[a] The E_{ads} in table is defined as $E_{ads} = E_{substrate} + E_{(WO_3)_3} - E_{(WO_3)_3/substrate}$ where $E_{substrate}$, $E_{(WO_3)_3}$ and $E_{(WO_3)_3/substrate}$ represent the total energies of clean defective MgO/Ag(100) films, the ground state of $(WO_3)_3$ cluster in the gas phase and the whole system for depositing $(WO_3)_3$ on defective MgO/Ag(100) films, respectively. [b] The negative values indicate that the electrons are transferred from the substrate to the $(WO_3)_3$ clusters.

adsorption on the defective MgO/Ag(001) films, the $(WO_3)_3$/defective-MgO/Ag(001) system exhibits reduced interface distances (about 2.59–2.66 Å away from the oxygen vacancy and 2.65–2.68 Å near the oxygen vacancy, respectively). While for the relaxation of top layer of the MgO films, significantly larger surface rumpling specially for Mg ions with obvious outward relaxation (about 0.30 Å) with respect to the surface plane are observed, resulting in the strengthening of Mg–O adsorption bonds, which provide a indication of the occurrence of negative charge accumulated on the adsorbed $(WO_3)_3$ clusters. Similar phenomena have been observed for the formation of other negatively charged species on the insulating MgO thin films.[31,34,41,59] In addition, we also consider the properties of $(WO_3)_3$ clusters supported on 2ML defective MgO ultrathin films supported on Ag(001). Compared with that adsorption on defective MgO(3ML)/Ag(001) films, the $(WO_3)_3$/defective-MgO(2ML)/Ag(001) exhibits similar structure with forming eight direct Mg–O bonds, but with slightly longer Mg–O bond lengths (2.10–2.30 Å), indicating weakened interaction between $(WO_3)_3$ clusters and the defective MgO(2ML)/Ag(001) films. Thus, corresponding adsorption energy (5.60 eV) is 0.24 eV lower in energy than that on the defective MgO(3ML)/Ag(001) films.

It is well known that MgO/Ag is a weakly bound interface. Van der Walls (vdW) forces are important for the description of the metal/oxide interface for the geometries and electronic properties. Now we consider the effect of vdW forces on the adsorption of $(WO_3)_3$ clusters on defective MgO ultrathin films using DFT-D2 method. With the inclusion of van der Waals corrections, the supported films exhibit smaller interface distances around the oxygen vacancy (0.14 Å, 0.17 Å for $(WO_3)_3$/defective-MgO(3ML)/Ag(001) and $(WO_3)_3$/defective-MgO(2ML)/Ag(001), respectively). And the adsorption energy is increased (about 28% and 31% for $(WO_3)_3$/defective-MgO(3ML)/Ag(001) and $(WO_3)_3$/defective-MgO(2ML)/Ag(001) system, respectively) as shown in Table 1.

3.2 Electronic structures of $(WO_3)_3$ clusters on the defective MgO ultrathin films supported on Ag(001)

Fig. 2 displays the partial density of states (DOSs) of the most stable configuration for $(WO_3)_3$ clusters deposited on the defective MgO ultrathin films supported on Ag(001). As shown in Fig. 2a, the Fermi level is determined by the Ag support, and falls in the gap of the defect MgO insulating films. An obvious and crucial feature with respect to this structure is that now two sharp peaks originated from the states of $(WO_3)_3$ clusters appear in the gap of the MgO insulating films. According to the atomic partial DOSs of W, O atoms of the supported clusters (Fig. 2b), we can further concluded that the new peak present about −1.5 eV below Fermi level is dominated by W 5d and O 2p states from the $(WO_3)_3$ clusters, and becomes occupied as a consequence of the interaction with the thin films. While another sharp peak at Fermi level mainly derives from one lowest W atom associated with the O_t atom that is used to heal the oxygen vacancy on the films. Moreover, charge density (Fig. 3b–c) further proves that the new isolated state at −1.5 eV below Fermi level is mainly localized around the W and O atoms of the $(WO_3)_3$ clusters, while the charge state around Fermi level is mainly localized around one lowest W atom associated with the O_t atom that is used to heal the oxygen vacancy on the films.

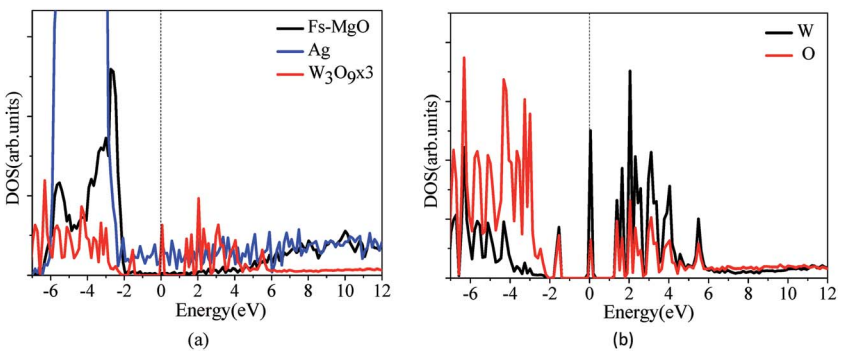

Fig. 2 (a and b) Particle DOSs, and partial DOSs projected on the W and O atoms of the clusters for the most stable configuration for $(WO_3)_3$ clusters deposited on the defective MgO ultrathin films supported on Ag(001), respectively. The vertical dashed line indicates the position of the Fermi level, taken as zero energy.

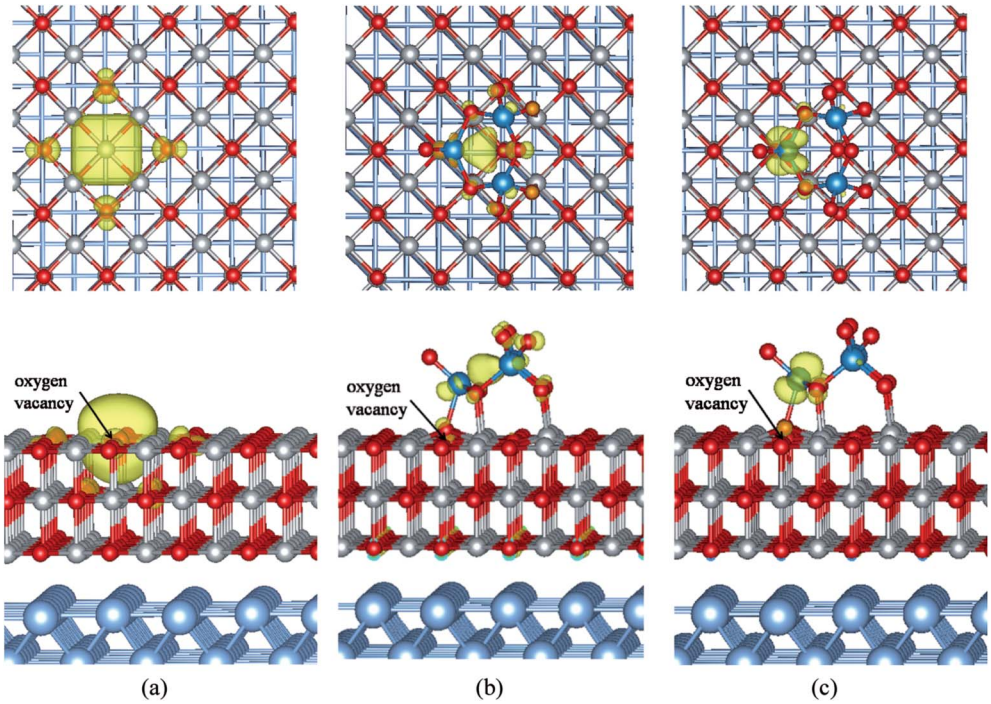

Fig. 3 The spin charge density for clean defective MgO ultrathin films supported on Ag(001) (a), charge density of the isolated state at −1.5 eV below Fermi level (b) and at Fermi level (c) for $(WO_3)_3$ clusters deposited on the defective MgO ultrathin films supported on Ag(001).

Now let us consider the charge transfers occurring between the $(WO_3)_3$ clusters and the defective MgO/Ag(001) films by analyzing the Bader charge distribution (Table 1). In here the negative value means the $(WO_3)_3$ clusters obtains electrons. We found a net charge transfer of 2.74*e* occurring from the defective MgO/Ag(001) films to the $(WO_3)_3$ clusters, which is more than that on the defect-free $(WO_3)_3$/MgO/Ag(001) system (1.87*e*)[34] and the thick defective MgO(001) surface (2.0*e*)[20] reported in previous results. Further analyses of Bader charge of atoms show that, the origin of this electron transfer is rather different, now the charge transfer occurs mainly directly from the Ag metal conduction band to $(WO_3)_3$ clusters through the MgO thin dielectric barrier (about 2*e*), and less charge transfer comes from the surface defective state by Mg–O dative bonds at interface (about 0.7*e*). In addition, the charge distributions within the $(WO_3)_3$ clusters are also further investigated. The results show that the W atom associated with the O_t atom healing the oxygen vacancy obtains the most of the electrons (0.83*e*), while other two W atoms get less electrons (about 0.25*e*, 0.25*e*, respectively), and other electrons are obtained by O atoms. However, it must be mentioned that, although there is obvious electron transfer from the defective MgO/Ag(001) films to $(WO_3)_3$ clusters, not all the electrons are obtained by W atoms, due to the unavoidable formation of bonds between the O atoms of clusters and the surface Mg atoms. Additionally, the charge transfer from the substrate to $(WO_3)_3$ clusters leads to the increase of work function (0.53 eV). In addition, when $(WO_3)_3$ clusters adsorption on the defective MgO(2ML)/Ag(001) films, the charge transfer is also large (2.69*e*), but slightly less than that in $(WO_3)_3$/defective-MgO(3ML)/Ag(001) (2.74*e*). Like the $(WO_3)_3$/defective-MgO(3ML)/Ag(001) system, the obtained electrons of adsorbed $(WO_3)_3$ clusters mainly originated from the spontaneous electron tunneling through the thin MgO dielectric barrier. Meanwhile, the analysis of Bader charge by Grimme's DFT-D2 method is also displayed in Table 1. It is obvious that the vdW interactions have no significant effects on the Bader charges, the difference being of 0.04–0.06*e*.

3.3 Observable properties

In this section, we will discuss two observable properties for the deposition of $(WO_3)_3$ clusters on the defective MgO ultrathin films supported on Ag(001) which can help in the identification of the formation of anionic $(WO_3)_3$ clusters in the future experiments. The first observable property is STM images, the second is vibrational spectra.

3.3.1 STM simulations. Using the Tersoff–Hamann approach, we have simulated STM images for the clean defective MgO ultrathin films supported on Ag(001), $V = -3.5$ V, the most stable structure of $(WO_3)_3$ clusters deposition on the defective MgO ultrathin films supported on Ag(001) at positive and negative bias, $V = +5.0$ V, +3.5 V, −5.0 V, −3.5 V, respectively (Fig. 4). Due to the well known DFT underestimate of the band gap in insulating materials, these values do not necessarily correspond to regions where tunneling occurs *via* empty or occupied states in direct measurements; these can, in fact, be typically shifted by 1–2 V compared to the computed regions.[62]

For the clean defective MgO ultrathin films supported on Ag(001), the simulated STM image with negative bias voltage is

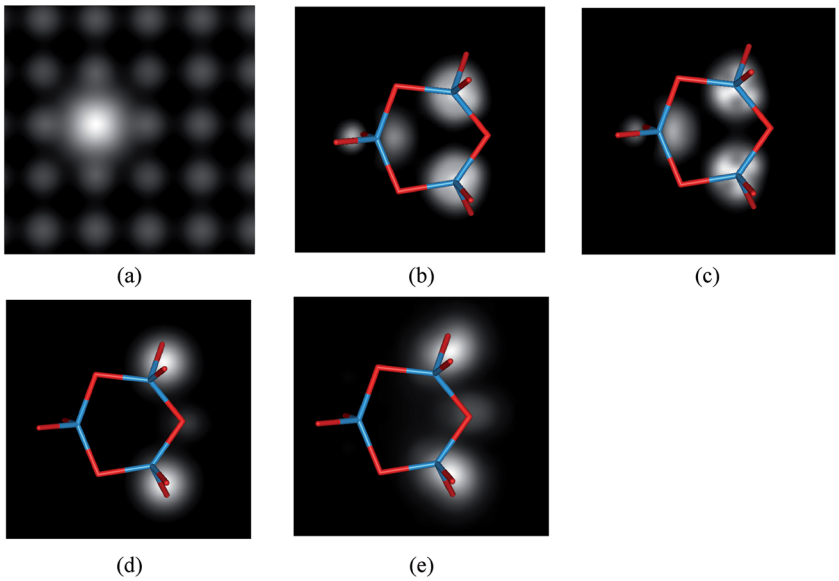

Fig. 4 Simulated STM images for the clean defective MgO ultrathin films supported on Ag(001) (a) $V = -3.5$ V, the most stable structure of $(WO_3)_3$ clusters deposition on the defective MgO/Ag(001) ultrathin films taken at different bias. (b) $V = +5.0$ V, (c) $V = +4.0$ V, (d) $V = -5.0$ V, (e) $V = -4.0$ V, respectively. An overlay of the $(WO_3)_3$ framework is also shown in picture (b–e).

shown in Fig. 4a. In the filled-state STM image, one protrusion are observed in the oxygen vacancy region clearly. While for the most stable structure of $(WO_3)_3$ clusters deposition on the defective MgO ultrathin films supported on Ag(001), we found that the best topographic images reflecting the cluster morphology are obtained at a positive bias voltage ($V = +5.0$ V) when tunneling into the W empty state takes place. Since the STM contrast is governed by the electronic properties and topographic position of the deposited $(WO_3)_3$ clusters. At the positive bias voltage, the brightest spots in the simulated STM images are mainly associated to the conductance spectra of W atoms with the higher position. The variation of the height of the W atoms in the deposited structures produces different distributions of the bright spots which reflect the irregular shape of the clusters. As shown in Fig. 4b and c, for the $(WO_3)_3$ clusters deposition on the defective MgO/Ag(001) films, at positive bias two brightest spots corresponding to the two W atoms at higher position and one less bright spot corresponding to the lowest W atom are observed. And a symmetric plane between the two brightest spots is found. This phenomenon is different from that previous reported for $(WO_3)_3$/perfect-MgO/Ag(001) films and $(WO_3)_3$/defective-MgO(001) surface, respectively. While at negative bias, the bridging and the terminal oxygens associated with the two W atoms at higher position become clearly visible in the simulated images (Fig. 4d and e).

3.3.2 Vibrational spectra. In this section, we will discuss another observable property, vibrational spectra, for the gas-phase $(WO_3)_3$ clusters and deposited $(WO_3)_3$ clusters on defective MgO/Ag(001) films. The vibrational properties for the free $(WO_3)_3$ clusters and most stable adsorption configuration are determined by using a central finite difference method, respectively. The corresponding intensities are obtained from the derivatives of the dipole moment, considering only the component perpendicular to the surface (surface selection rule) for the deposited clusters (namely, the surface selection rule applied in the high-resolution electron energy loss spectroscopy).[63]

For the gas-phase $(WO_3)_3$ clusters (Fig. 5a), the peak located at 834 cm^{-1} can be assigned to W–O_b–W mode. While W–O_t double bonds produced peaks at higher frequencies centered at 979, 1025 cm^{-1}. These values are in good agreement with the experimental frequencies reported for the gas-phase $(WO_3)_3$ nanoclusters, 859, 975, and 1014 cm^{-1}.[64] While for the $(WO_3)_3$ clusters adsorption on the defective MgO/Ag(001) films, the vibrational spectrum becomes considerably more complex compared to gas-phase $(WO_3)_3$ clusters, due to the distortion of the supported $(WO_3)_3$ clusters (Fig. 5b). According to the coordinations of the O atoms (Fig. 1c), they can be divided into four groups, including the O_t and O_b atoms that are still at the terminal positions and bridge positions, and the O_t and O_b atoms that are connected with surface Mg atoms denoted by O'_t and O'_b, respectively. As displayed in Fig. 5b, two peaks related to the W–O_t bonds at 1007 and 974 cm^{-1} are almost unchanged, compared to that in gas-phase $(WO_3)_3$ clusters (979 cm^{-1}, 1025 cm^{-1}). While another peaks at 863 cm^{-1} and 857 cm^{-1}, related to the stretching modes of W–O'_t bonds involved in a bond with the surface are redshifted (120–160 cm^{-1}), due to the elongation of W–O'_t bond (about 0.1–0.3 Å) compared to that in gas phase (see Fig. 1c). We also observed the obvious redshifts of the W–O'_b–W modes, which now show peaks at 630, 671, 716 cm^{-1}, respectively. This is because the obvious elongation of W–O'_b bonds (about 0.07 Å) of O_b atom bonded with the surface Mg atoms.

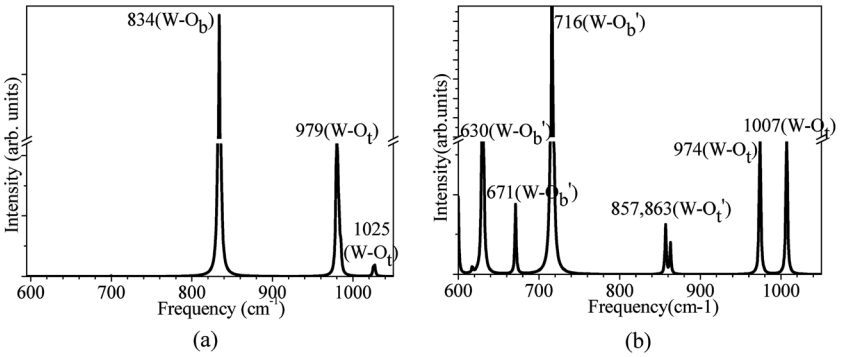

Fig. 5 Computed IR spectra for (a) gas-phase $(WO_3)_3$ clusters, (b) $(WO_3)_3$ clusters deposited on the defective MgO ultrathin films supported on Ag(001). A schematic assignment to specific vibrational modes is given in the spectra. The terminal oxygens and bridge oxygens in $(WO_3)_3$ clusters are denoted as O'_t and O'_b when bound to the MgO surface, respectively.

4. Conclusions

In the present work, the atomic structures and electronic properties of $(WO_3)_3$ nanoclusters adsorption on the defective MgO ultrathin films supported on Ag(001) have been systematically investigated by first-principles DFT calculations. Our results show that, after deposition, the oxygen vacancy on the defective MgO/Ag(001) films is healed by one terminal oxygen atom of the $(WO_3)_3$ clusters through forming four O–Mg bonds. The conformation of $(WO_3)_3$ nanoclusters is distorted slightly and the W_3O_3 cyclic conformation of adsorbed $(WO_3)_3$ nanoclusters is still maintained. The defective MgO/Ag(001) 2D films lead to enhance adsorption energy (5.84 eV) between the $(WO_3)_3$ clusters and the substrates, compared to that on the defect-free MgO/Ag(001) 2D films (3.48 eV) and the defective MgO(001) surface (5.76 eV). It is interesting that obvious charge transfer (2.74*e*) occurs from the defective MgO/Ag(001) films to the 5d empty state of $(WO_3)_3$ clusters that fall below the Ag Fermi level, which is more than that on the defect-free $(WO_3)_3$/MgO/Ag(001) system (1.87*e*) and the thick defective MgO(001) surface (2.0*e*) reported in previous works. Furthermore, the extent and origin of this electron transfer is rather different. For the $(WO_3)_3$/defective MgO/Ag(001) films, two extra electrons are coming directly from the Ag metal conduction band to $(WO_3)_3$ clusters by a spontaneous electron tunneling mechanism through the MgO thin dielectric barrier, and about 0.7*e* transfer comes from the surface defective state as the consequence of the formation of Mg–O dative bonds at interface. In addition, the different scanning tunneling microscopy images and vibrational spectra of deposited $(WO_3)_3$ nanoclusters are compared with those of the $(WO_3)_3$ nanoclusters in gas phase, defect-free MgO/Ag(001) 2D films and the defective MgO(001) surface, which can help in the identification of $(WO_3)_3$ nanoclusters adsorption on the defective MgO/Ag(001) ultrathin films in future experiments. In conclusion, both results reveal that $(WO_3)_3$ nanoclusters adsorption on the defective MgO/Ag(001) ultrathin films provides a new avenue to tune and modify the charge state and chemical reactivity of tungsten oxide nanoclusters as a function of the thickness of the supporting oxide films. Finally, it must be mentioned that, since the oxygen vacancies form preferentially at low-coordinated sites (such as steps, edges, and corners) on the MgO films may effect the electronic properties of the MgO films and the adsorbed clusters. Further works are necessary to study the changes of the structures and the charge states when $(WO_3)_3$ clusters are adsorbed on the defective MgO ultra-thin films with O vacancies at low-coordinated sites.

Conflicts of interest

There are no conflicts to declare.

Acknowledgements

This work was supported by National Natural Science Foundation of China (Grant No. 21403094, 21373048, 21666020), Special Program for Applied Research on Super Computation of the NSFC-Guangdong Joint Fund (the second phase) under Grant No. U1501501, the Independent Research Project of State Key Laboratory of Photocatalysis on Energy and Environment (No. 2014A02). We are grateful for the generous allocation of computer time on the National Supercomputer Center in Guangzhou houses Tianhe-2.

References

1 B. L. Yoder, J. T. Maze, K. Raghavachari and C. C. Jarrold, *J. Chem. Phys.*, 2005, **122**, 094313.
2 Q. Sun, B. K. Rao, P. Jena, D. Stolcic, Y. D. Kim, G. Gantefor and A. W. Castleman, *J. Chem. Phys.*, 2004, **121**, 9417.
3 L. Q. Mai, W. L. Guo, B. Hu, W. Jin and W. Chen, *J. Phys. Chem. C*, 2008, **112**, 423–429.
4 R. Rousseau, D. A. Dixon, B. D. Kaya and Z. Dohnáleka, *Chem. Soc. Rev.*, 2014, **43**, 7664–7680.
5 R. D. Wilson, D. G. Barton, C. D. Baertsch and E. Iglesia, *J. Catal.*, 2000, **194**, 175–187.
6 W. Grunert, R. Feldhaus, K. Anders, E. S. Sphiro and K. M. Minachev, *J. Catal.*, 1989, **120**, 444–456.
7 C. Martin, G. Solana, P. Malet and V. Rives, *Catal. Today*, 2003, **78**, 365–376.

8 L. Lietti, J. L. Alemany, P. Forzatti, G. Busca, G. Ramis, E. Giamello and F. Bregani, *Catal. Today*, 1996, **29**, 143–148.
9 O. Bondarchuk, X. Huang, J. Kim, B. D. Kay, L. S. Wang, J. M. White and Z. Dohnálek, *Angew. Chem., Int. Ed.*, 2006, **45**, 4786–4789.
10 Y. K. Kim, R. Rousseau, B. D. Kay, J. M. White and Z. Dohnálek, *J. Am. Chem. Soc.*, 2008, **130**, 5059–5061.
11 M. Wagner, S. Surnev, M. G. Ramsey, G. Barcaro, L. Sementa, F. R. Negreiros, A. Fortunelli, Z. Dohnálek and F. P. Netzer, *J. Phys. Chem. C*, 2011, **115**, 23480–23487.
12 S. C. Li, Z. Li, Z. Zhang, B. D. Kay, R. Rousseau and Z. Dohnálek, *J. Phys. Chem. C*, 2012, **116**, 908–916.
13 Y. K. Kim, R. Rousseau, B. D. Kay, J. M. White and Z. Dohnálek, *J. Am. Chem. Soc.*, 2008, **130**, 5059–5061.
14 Y. K. Kim, Z. Dohnálek, B. D. Kay and R. Rousseau, *J. Phys. Chem. C*, 2009, **113**, 9721–9730.
15 J. Kim, B. D. Kay and Z. Dohnálek, *J. Phys. Chem. C*, 2010, **114**, 17017–17022.
16 Z. J. Li, Z. R. Zhang, B. D. Kay and Z. Dohnálek, *J. Phys. Chem. C*, 2011, **115**, 9692–9700.
17 H.-J. Freund, *Surf. Sci.*, 2007, **601**, 1438–1442.
18 H.-J. Freund and G. Pacchioni, *Chem. Soc. Rev.*, 2008, **37**, 2224–2242.
19 C. Di Valentin, M. Rosa and G. Pacchioni, *J. Am. Chem. Soc.*, 2012, **134**, 14086–14098.
20 J. Zhu, S. J. Lin, X. W. Wen, Z. X. Fang, Y. Li, Y. F. Zhang, X. Huang, L. X. Ning, K. N. Ding and W. K. Chen, *J. Chem. Phys.*, 2013, **138**, 034711.
21 H. Y. T. Chen and G. Pacchioni, *Phys. Chem. Chem. Phys.*, 2014, **16**, 21838–21845.
22 F. Ringleb, Y. Fijimori, M. A. Brown, W. E. Kaden, F. Calaza, H. Kuhlenbeck, M. Sterrer and H.-J. Freund, *Catal. Today*, 2015, **240**, 206–213.
23 H.-J. Freund and D. W. Goodman, Ultrathin oxide films, *Handbook of Heterogeneous Catalysis*, 2008, p. 1309.
24 A. K. Santra and D. W. Goodman, Oxide-supported metal clusters: models for heterogeneous catalysts, *J. Phys.: Condens. Matter*, 2002, **14**, R31–R62.
25 H.-J. Freund and G. Pacchioni, *Chem. Soc. Rev.*, 2008, **37**, 2224–2242.
26 S. M. McClure and D. W. Goodman, *Top. Catal.*, 2011, **54**, 349–362.
27 G. Pacchioni, *Chem.–Eur. J.*, 2012, **18**, 10144–10158.
28 J. Pal, M. Smerieri, E. Celasco, L. Savio, L. Vattuone, R. Ferrando, S. Tosoni, L. Giordano, G. Pacchioni and M. Rocca, *J. Phys. Chem. C*, 2014, **118**, 26091–26102.
29 S. Sicolo, L. Giordano and G. Pacchioni, *J. Phys. Chem. C*, 2009, **113**, 16694–16701.
30 G. Pacchioni, *Phys. Chem. Chem. Phys.*, 2013, **15**, 1737–1757.
31 L. Giordano and G. Pacchioni, *Acc. Chem. Res.*, 2011, **44**, 1244–1252.
32 G. Pacchioni, L. Giordano and M. Baistrocchi, *Phys. Rev. Lett.*, 2005, **94**, 226104.
33 S. Sicolo, L. Giordano and G. Pacchioni, *J. Phys. Chem. C*, 2009, **113**, 10256–10263.
34 J. Zhu, L. Giordano, S. J. Lin, Z. X. Fang, Y. Li, X. Huang, Y. F. Zhang and G. Pacchioni, *J. Phys. Chem. C*, 2012, **116**, 17668–17675.
35 H. Grönbeck, *J. Phys. Chem. B*, 2006, **110**, 11977–11981.
36 M. Sterrer, T. Risse, U. M. Pozzoni, L. Giordano, M. Heyde, H.-P. Rust, G. Pacchioni and H.-J. Freund, *Phys. Rev. Lett.*, 2007, **98**, 096107.
37 M. Yulikov, M. Sterrer, M. Heyde, H.-P. Rust, T. Risse, H.-J. Freund, G. Pacchioni and A. Scagnelli, *Phys. Rev. Lett.*, 2006, **96**, 146804.
38 V. Simic-Milosevic, M. Heyde, N. Nilius, T. König, H.-P. Rust, M. Sterrer, T. Risse, H.-J. Freund, L. Giordano and G. Pacchioni, *J. Am. Chem. Soc.*, 2008, **130**, 7814–7815.
39 X. Lin, N. Nilius, H.-J. Freund, M. Walter, P. Frondelius, K. Honkala and H. Häkkinen, *Phys. Rev. Lett.*, 2009, **102**, 206801.
40 C. Zhang, B. Yoon and U. Landman, *J. Am. Chem. Soc.*, 2007, **129**, 2228–2229.
41 A. Gonchar, T. Risse, H.-J. Freund, L. Giordano, C. Di Valentin and G. Pacchioni, *Angew. Chem., Int. Ed.*, 2011, **50**, 2635–2638.
42 P. Frondelius, A. Hellman, K. Honkala, H. Häkkinen and H. Grönbeck, *Phys. Rev. B: Condens. Matter Mater. Phys.*, 2008, **78**, 085426.
43 G. Kresse and J. Hafner, *Phys. Rev. B: Condens. Matter Mater. Phys.*, 1993, **47**, 558–561.
44 G. Kresse and J. Hafner, *Phys. Rev. B: Condens. Matter Mater. Phys.*, 1994, **49**, 14251–14269.
45 G. Kresse and J. Furthmüller, *Comput. Mater. Sci.*, 1996, **6**, 15–50.
46 P. E. Blöchl, *Phys. Rev. B: Condens. Matter Mater. Phys.*, 1994, **50**, 17953–17979.
47 J. Hafner, *J. Comput. Chem.*, 2008, **29**, 2044–2078.
48 J. P. Perdew and Y. Wang, *Phys. Rev. B: Condens. Matter Mater. Phys.*, 1992, **45**, 13244–13249.
49 S. Grimme, *J. Comput. Chem.*, 2006, **27**, 1787–1799.
50 S. Li and D. A. Dixon, *J. Phys. Chem. A*, 2006, **110**, 6231–6244.
51 S. Li and D. A. Dixon, *J. Phys. Chem. A*, 2007, **111**, 11093–11099.
52 X. Huang, H.-J. Zhai, J. Li and L.-S. Wang, *J. Phys. Chem. A*, 2001, **106**, 85–92.
53 U. Martinez, G. Pacchioni and F. Illas, *J. Chem. Phys.*, 2009, **130**, 184711.
54 A. Del Vitto, C. Sousa, F. Illas and G. Pacchioni, *J. Chem. Phys.*, 2004, **121**, 7457–7466.
55 L. B. Vilhelmsen and B. Hammer, *Phys. Rev. Lett.*, 2012, **108**, 126101.
56 S. Nosé, *J. Chem. Phys.*, 1984, **81**, 511–519.
57 J. Zhu, H. Jin, L. L. Zang, Y. Li, Y. F. Zhang, K. N. Ding, X. Huang, L. X. Ning and W. K. Chen, *J. Phys. Chem. C*, 2011, **115**, 15335–15344.
58 J. Zhu, H. Jin, W. J. Chen, Y. Li, Y. F. Zhang, L. X. Ning, X. Huang, K. N. Ding and W. K. Chen, *J. Phys. Chem. C*, 2009, **113**, 17509–17517.
59 J. Zhu, H. Zhang, L. Zhao, W. Xiong, X. Huang, B. Wang and Y. F. Zhang, *Appl. Surf. Sci.*, 2016, **379**, 213–222.

60 S. Prada, U. Martinez and G. Pacchioni, *Phys. Rev. B: Condens. Matter Mater. Phys.*, 2008, **78**, 235423.
61 S. L. Ling, M. B. Watkins and A. L. Shluger, *Phys. Chem. Chem. Phys.*, 2013, **15**, 19615–19624.
62 N. Nilius, *Surf. Sci. Rep.*, 2009, **64**, 595–659.
63 M. Preuss and F. Bechstedt, *Phys. Rev. B: Condens. Matter Mater. Phys.*, 2006, **73**, 155413.
64 Z. J. Li, Z. R. Zhang, Y. K. Kim, R. S. Smith, F. Netzer, B. D. Kay, R. Rousseau and Z. Dohnálek, *J. Phys. Chem. C*, 2011, **115**, 5773–5783.